ACS OMEGA

http://pubs.acs.org/journal/acsodf

Article

Light-Induced Wavelength Dependent Self Assembly Process for Targeted Synthesis of Phase Stable 1D Nanobelts and 2D Nanoplatelets of $CsPbI_3$ Perovskites

Avijit Pramanik, Sudarson Sekhar Sinha, Kaelin Gates, Jing Nie, Fengxiang X Han, and Paresh Chandra Ray*

Cite This: *ACS Omega* 2023, 8, 13202−13212

Read Online

ACCESS | Metrics & More | Article Recommendations | Supporting Information

ABSTRACT: Despite black cubic phase α-$CsPbI_3$ nanocrystals having an ideal bandgap of 1.73 eV for optoelectronic applications, the phase transition from α-$CsPbI_3$ to non-perovskite yellow δ-$CsPbI_3$ phase at room temperature remains a major obstacle for commercial applications. Since γ-$CsPbI_3$ is thermodynamically stable with a bandgap of 1.75 eV, which has great potential for photovoltaic applications, herein we report a conceptually new method for the targeted design of phase stable and near unity photoluminescence quantum yield (PLQY) two-dimensional (2D) γ-$CsPbI_3$ nanoplatelets (NPLs) and one-dimensional (1D) γ-$CsPbI_3$ nanobelts (NBs) by wavelength dependent light-induced assembly of $CsPbI_3$ cubic nanocrystals. This article demonstrates for the first time that by varying the excitation wavelengths, one can design air stable desired 2D nanoplatelets or 1D nanobelts selectively. Our experimental finding indicates that 532 nm green light-driven self-assembly produces phase stable and highly luminescent γ-$CsPbI_3$ NBs from $CsPbI_3$ nanocrystals. Moreover, we show that a 670 nm red light-driven self-assembly process produces stable and near unity PLQY γ-$CsPbI_3$ NPLs. Systematic time-dependent microscopy and spectroscopy studies on the morphological evolution indicates that the electromagnetic field of light triggered the desorption of surface ligands from the nanocrystal surface and transformation of crystallographic phase from α to γ. Detached ligands played an important role in determining the morphologies of final structures of NBs and NPLs from nanocrystals via oriented attachment along the [110] direction initially and then the [001] direction. In addition, XRD and fluorescence imaging data indicates that both NBs and NPLs exhibit phase stability for more than 60 days in ambient conditions, whereas the cubic phase α-$CsPbI_3$ nanocrystals are not stable for even 3 days. The reported light driven synthesis provides a simple and versatile approach to obtain phase pure $CsPbI_3$ for possible optoelectronic applications.

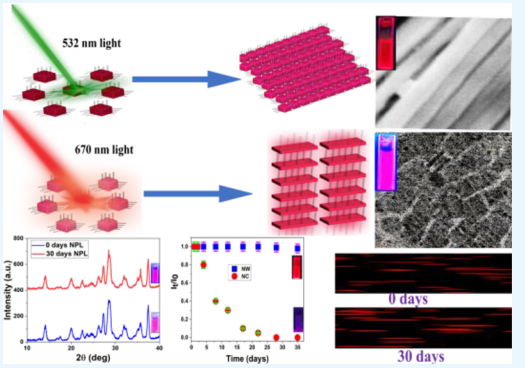

1. INTRODUCTION

Due to the high photoluminescence quantum yield (PLQY) and a tunable bandgap, all-inorganic cesium lead halide perovskite ($CsPbX_3$, where X can be Cl^-, Br^-, or I^-) nanocrystals are highly suitable for next generation optoelectronic applications.[1−10] Among them, cubic phase α-$CsPbI_3$ nanocrystals have an ideal bandgap of 1.73 eV for solar cells and near-unity PLQY for light-emitting diode (LED) applications.[11−20]

Despite $CsPbI_3$ perovskites being most promising candidates, the poor phase stability due the room temperature transition from cubic-phase α-$CsPbI_3$ ($E_{bandgap}$ = 1.73 eV) to a non-perovskite δ-$CsPbI_3$ phase ($E_{bandgap}$ = 2.25 eV) with weak response to the solar spectrum remains a major obstacle for the commercial application.[21−30] In the case of all-inorganic cesium lead iodide perovskite, the α-phase is intrinsically unstable, which is due to several factors such as surface iodide vacancies and poor surface capping ligands.[11−20,30−41] Furthermore, the Cs^+ ions in cubic α-$CsPbI_3$ are not large enough to stabilize the cubic framework of corner-sharing $[PbI_6]^{4-}$ octahedra, which allow distortion via dynamic motion.[9−16] As a result, $CsPbI_3$ perovskite undergoes phase transition between four phases, and those are cubic structure (α) which is only stable over 330 °C, the tetragonal structure (β) which is stable around 200 °C, and two orthorhombic structures (γ and δ), which are stable at room temperature.[9−20] It has been well documented that the γ- and δ-phases of $CsPbI_3$ perovskite are thermodynamically favored at room temperature and α- and β-phases are stable at high temperature.[11−20] However, the δ-$CsPbI_3$ phase ($E_{bandgap}$ =

Received: January 24, 2023
Accepted: March 15, 2023
Published: March 31, 2023

2.25 eV) with poor photoluminescence quantum yield (PLQY) is not good for photovoltaic applications. On the other hand, γ-$CsPbI_3$ is thermodynamically stable and has a bandgap of 1.75 eV, which has great potential for photovoltaic applications.[11−20] To overcome the phase stability problem, in the current article, we report a conceptually new method for the targeted design of phase stable and near unity PLQY two-dimensional (2D) γ-$CsPbI_3$ nanoplatelets (NPLs) and one-dimensional (1D) γ-$CsPbI_3$ nanobelts (NBs) by wavelength dependent visible light-induced assembly of $CsPbI_3$ nanocrystals.

Light-induced noncovalent interaction based self-assembly of desired organized structures is one of the most facile approaches for achieving highly ordered superlattice structures.[1−10] It is now well documented that noncovalent interaction based self-assembly is an effective strategy for constructing long-range order nanostructures with less defects.[1−10]

Due to the stronger quantum confinement effects compared to the $CsPbX_3$ nanocrystals, nanoplatelets, nanorods, and nanobelts have higher photon absorption cross sections, enhanced photovoltaic efficiencies, and improved charge-carrier transport.[21−41] As a result, design of perovskite assemblies of 1D and 2D nanostructures using the bottom-up self-assembly strategy has stimulated huge interest.[1−10] Due to the above fact, several groups have attempted the development of $CsPbI_3$ nanowires via the solvent assisted synthesis method or hot injection method.[12−15,25]

Reported data show that developing phase stable $CsPbI_3$ nanowires is challenging since they spontaneously convert to δ-$CsPbI_3$.[13,14] Driven by the need, in this article, we report that a light-induced noncovalent interaction based self-assembly process can be used as a facile approach for achieving phase pure, highly luminescent γ-$CsPbI_3$ NBs and NPLs which are stable at room temperature for several weeks. Reported data show that the targeted design of 2D nanoplatelets and 1D nanobelts can be manipulated by varying the wavelength of excitation light as shown in Figure 1. Systematic time-dependent microscopy and spectroscopy studies on the morphological evolution indicate that the electromagnetic field of the laser light induces a dipole on the α-$CsPbI_3$ via desorption of surface ligands and transformation of the crystallographic phase, which allow hierarchical self-assembly of $CsPbI_3$ nanocrystals into different structures through oriented attachment via dipole−dipole interactions.

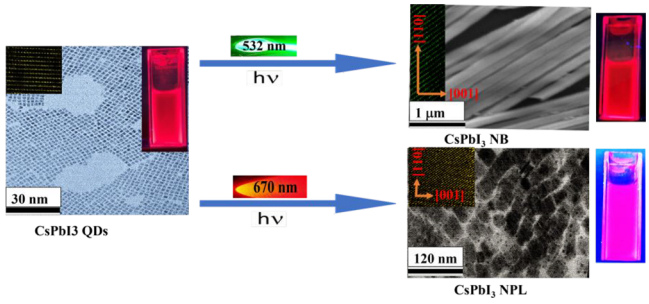

Figure 1. Photograph under UV light and TEM and HRTEM images show the development of two-dimensional γ-$CsPbI_3$ nanoplatelets and one-dimensional γ-$CsPbI_3$ nanobelts by red and green light-induced assembly of $CsPbI_3$ cubic nanocrystals.

2. RESULTS AND DISCUSSIONS

2.1. Synthesis, Characterization, and Photochemistry of α-$CsPbI_3$ Cubic Nanocrystals. The highly crystalline, large grain size cesium lead iodide perovskite nanocrystals were synthesized by following a previous literature procedure with slight modification.[31,32] In brief, the Cs-oleate precursor solution was first prepared by loading Cs_2CO_3 (0.8 g) into oleic acid (OA) (2.5 mL) and 1-octadecene (ODE) (30 mL) in the round-bottom flask at 120 °C and then continuously heating under the flow of N_2 gas in the oil bath until all Cs_2CO_3 was dissolved completely.[32] At the same time, 0.171 g PbI_2 was loaded into another 50 mL round-bottom flask with 10 mL ODE and dried under vacuum for 2 h at 120 °C.[32] Then 1 mL oleylamine (OAm) and 1 mL OA were immediately injected into the flask at 120 °C until the mixture was completely dissolved and the temperature of the solution was increased to 180 °C.

Next, 1 mL of the as prepared Cs-oleate solution was quickly injected into the flask After reacting for 30 s, the reaction mixture was cooled to room temperature using an ice−water bath. The freshly prepared perovskite nanocrystals were then precipitated by centrifugation with hexane for 5 min at 8000 rpm. Then, the supernatant was discarded, and the obtained precipitate was again redispersed in hexane at 4 °C. At the end, $CsPbI_3$ nanocrystals were characterized using tunneling electron microscopy (TEM) (Figures 1 and 2) and dynamic light scattering (DLS).[26,31,32] As reported in Table 1, the DLS data indicates that the size is around 6 ± 1 nm. TEM data reported in Figure 2A indicates that the size is around 5 ± 1 nm, which matches quite well with DLS data.

Energy-dispersive X-ray (EDX) spectroscopy (Figure S1 in Supporting Information) and inductively coupled plasma mass spectrometer (ICP-MS) data indicate that the nanocrystals are $CsPbI_3$. The HRTEM image, as shown in the inset image of Figure 1, shows clear lattice fringes with interplanar spacing (d) of ∼0.31 nm which is due to the (100) crystal plane of α-$CsPbI_3$.[12,13,15,19] The X-ray powder diffraction (XRD) data from α-$CsPbI_3$ reported in Figure 3E shows (100) and (200) planes (JCPDS No. 80-4039). Figure 3G shows the FTIR spectra from $CsPbI_3$ nanocrystals, which show a strong peak at 1535 cm^{-1}, which is due to the $-COO^-$ from oleate anions. Similarly, we have also observed a strong peak at 3310 cm^{-1}, which is due to $-NH_2$ group from oleyl amine (OAm), and another peak at 1635 cm^{-1}, which is due to $-NH_3^+$ from protonated amine.

Figure 3A1 shows the photograph of α-$CsPbI_3$ in the absence of UV light. Figure 3B1 shows the photograph of α-$CsPbI_3$ in the presence of UV light, which clearly shows strong red luminescence. Figure 3D shows the luminescence spectra from α-$CsPbI_3$, which indicates that the λ_{max} of freshly prepared nanocrystals is 716 nm (1.73 eV). We have calculated the photoluminescence quantum yield (PLQY) using eq 1.[26,31,32]

$$\mathrm{PLQY} = N_{\mathrm{emit}}/N_{\mathrm{absorb}} \quad (1)$$

where N_{emit} and N_{absorb} are the number of emitted and absorbed photons, respectively, for α-$CsPbI_3$. Using our experimental data and eq 1, we estimated that the photoluminescent quantum yield for α-$CsPbI_3$ nanocrystals is ∼88%, which is comparable with literature published data.[7,12−16]

2.2. 532 nm Green Light Driven Synthesis, Characterization, and Photochemistry of γ-$CsPbI_3$ Nanobelts

https://doi.org/10.1021/acsomega.3c00477
ACS Omega 2023, 8, 13202−13212

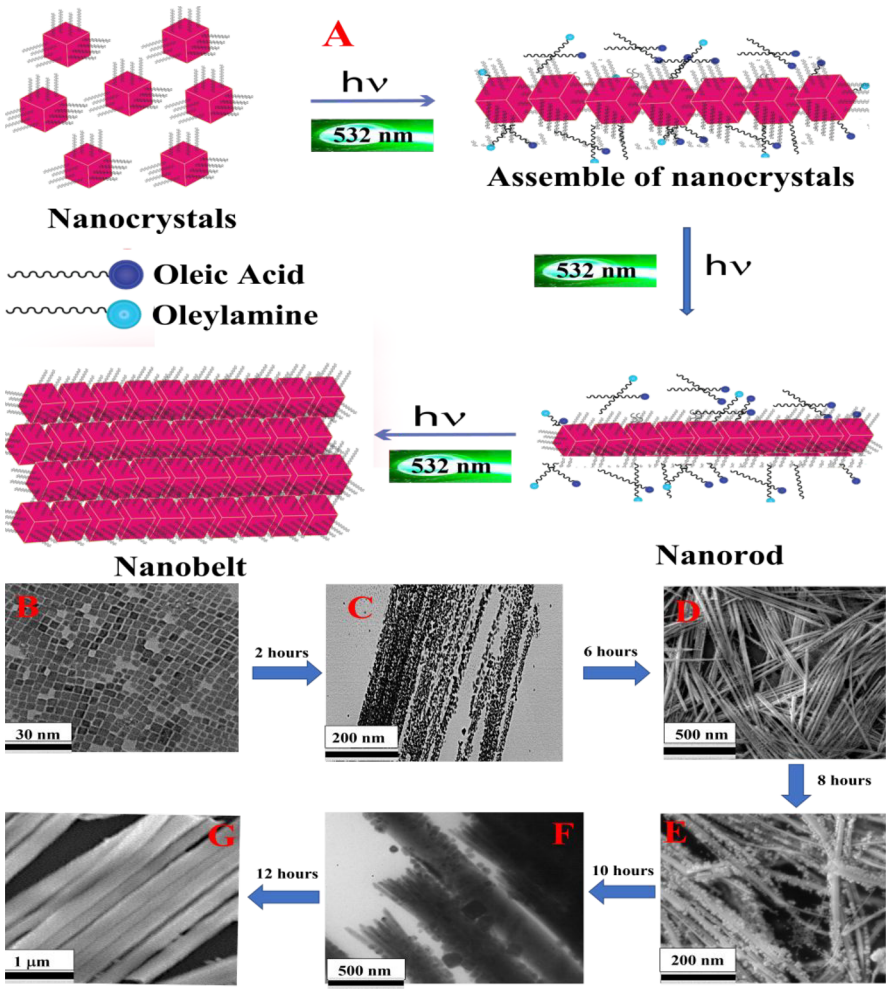

Figure 2. (A) Scheme of the 532 nm green light-induced evolution process from $CsPbI_3$ nanocrystals to γ-$CsPbI_3$ nanobelt. (B–G) Time-dependent TEM and SEM study showing the evidence of evolution process from cubic nanocrystals to nanobelt in the presence of 532 nm green light: (B) 0 h, (C) 2 h, (D) 6 h, (E) 8 h, (F) 10 h, and (G) 12 h.

Table 1. Size of $CsPbI_3$ Perovskite Measured by DLS and TEM Images

morphology	DLS data	TEM data
nanocrystals	6 ± 1 nm	5 ± 1 nm
nanobelt		length = 10 ± 4 μm, thickness = 250 ± 40 nm
nanoplatelets	length = 20 ± 8 nm, thickness = 4 ± 1 nm	length = 20 ± 6 nm, thickness = 4 ± 1 nm

from α-$CsPbI_3$ Quantum Dots. For light driven synthesis of nanobelts from nanocrystals, we have used a 532 nm diode-pumped solid state (DPSS) laser as the light source. For this experiment, we used 100 mW/cm^2 laser power for the development of NBs via the assembly process from $CsPbI_3$ nanocrystals. As shown in Figure 2, upon exposure to 532 nm light for several hours, $CsPbI_3$ nanocrystals change into a 1D nanowire initially and then from the nanowire to nanobelts. As shown in Figure 2G, the TEM data indicate that the size of the 1D $CsPbI_3$ nanobelts are around 10 ± 4 μm in length and 200 ± 40 nm in diameter. Energy-dispersive X-ray (EDX) spectroscopy (Figure S2 in Supporting Information) and inductively coupled plasma mass spectrometer (ICP-MS) data indicate that the NBs are $CsPbI_3$. X-ray diffraction (XRD) data, as reported in Figure 3F, shows (110), (112), (120), (212), (004), (220), (130), (132), and (224) planes for NBs, which indicates orthorhombic phase for γ-$CsPbI_3$ nanobelts (JCPDS No. 18-0376)[11−13] From XRD data reported in Figure 3E,F, we can clearly see that the phase changes from α-$CsPbI_3$ nanocrystals to γ-$CsPbI_3$ nanobelts. Similarly, the HRTEM image, as shown in the inset image of Figure 1 shows clear lattice fringes with interplanar spacing (d) of ∼0.28 nm which is due to the (220) crystal plane of γ-$CsPbI_3$.[11−13] Figure 3A2 shows the photograph of γ-$CsPbI_3$ nanobelts in the absence of UV light. Figure 3B1 shows the photograph of γ-$CsPbI_3$ nanobelts in the presence of UV light, which clearly shows strong red luminescence. Figure 3D shows the luminescence spectra from γ-$CsPbI_3$ nanobelts, which indicates λ_{max} of freshly prepared NB is 708 nm (1.75 eV). From the emission spectra of $CsPbI_3$ nanocrystals and 1D $CsPbI_3$ NBs, we can clearly observe a slight blue shift of photoluminescence λ_{max} from 716 to 708 nm. The observed slight blue shift of photoluminescence λ_{max} for γ-$CsPbI_3$ nanobelts compared with the $CsPbI_3$ nanocrystals can be due to the transformation from α-$CsPbI_3$ to γ-$CsPbI_3$, as well as the quantum confinement in one direction for nanobelts.[20−30] The photoluminescence quantum yield measurement shows PLQY increases from 88% to 92% after self-assembly formation from $CsPbI_3$ nanocrystals to γ-$CsPbI_3$ nanobelts. As we have observed in the SEM/TEM images reported in Figure 2, the close packed

https://doi.org/10.1021/acsomega.3c00477
ACS Omega 2023, 8, 13202−13212

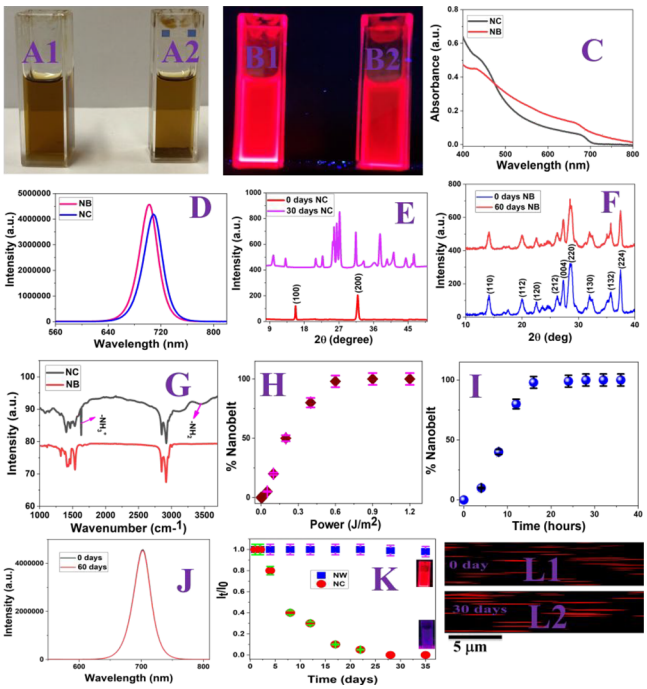

Figure 3. (A1) Photograph of $CsPbI_3$ nanocrystals in the absence of UV light. (A2) Photograph of $CsPbI_3$ NBs in the absence of UV light. (B1) Photograph of $CsPbI_3$ nanocrystals in the presence of UV light. (B2) Photograph of $CsPbI_3$ NBs in the presence of UV light. (C) UV−vis absorption spectra of $CsPbI_3$ nanocrystals and NBs. (D) Photoluminescence spectra of $CsPbI_3$ nanocrystals and NBs. (E) X-ray diffraction patterns from $CsPbI_3$ nanocrystals after fresh synthesis show α-$CsPbI_3$ (JCPDS No. 80-4039), and those after storage for 30 days show δ-$CsPbI_3$ (JCPDS 01-076-8588). (F) X-ray diffraction patterns from $CsPbI_3$ NBs after fresh synthesis and storage for 60 days show γ-$CsPbI_3$ (JCPDS No. 18-0376) in both cases. (G) FTIR spectra from $CsPbI_3$ nanocrystals and $CsPbI_3$ NBs, which indicate that the IR band from $-NH_2$ and $-NH_3^+$ disappears upon ligand desorption. (H) Plot shows the variation of % of $CsPbI_3$ NB formation with the power (J/m^2) of 532 nm visible light used for the experiment. For each laser power, we performed the experiment for 24 h. The percentage of nanobelts after the 24 h light exposure was measured using SEM, TEM, DLS, and luminescence data. The experiment was performed five times, and error bars were calculated from the standard deviation. (I) Plot shows the variation of % of $CsPbI_3$ NB formation with time during the 532 nm light-induced self-assembly process. The percentage of nanobelts after light exposure was measured using SEM, TEM, DLS, and luminescence data. The experiment was performed five times, and error bars were calculated from the standard deviation. (J) Photoluminescence spectra of $CsPbI_3$ NBs at 0 and 60 days. (K) Plot shows how the luminescence intensity from $CsPbI_3$ nanocrystals and $CsPbI_3$ NBs varies with the time of air exposure. The experiment was performed five times, and error bars were calculated from the standard deviation. (L1) Fluorescence microscopic images of $CsPbI_3$ NBs after fresh synthesis. (L2) Fluorescence microscopic images of $CsPbI_3$ NBs after 60 day storage.

arrangement of nanocrystals inside the nanowire via certain disorder, which can help localization of excitons in the local potential minima.[20−30] As a result, the traps formed in the presence of light, may not heavily involve recombination processes, which enhances PLQY for γ-$CsPbI_3$ nanobelts compared to $CsPbI_3$ nanocrystals.[20−30] To understand better, we have measured photoluminescence lifetimes for nanocrystals and nanowires, as reported in Figure S3A and Table S1A in the Supporting Information. Reported photoluminescence lifetime data indicate that for nanocrystals, the photoluminescence carrier lifetime is ∼3 ns and, on the other hand, for nanowires the photoluminescence carrier lifetime is ∼105 ns. This observed longer photoluminescence carrier lifetime for nanowires in comparison to nanocrystals indicates effective suppression of nonradiative traps for nanowire and it also indicates long carrier diffusion length for nanowires.[20−30] So experimentally observed higher PLQY for assembled structures can be due to the low trap density, as well as strong quantum confinement.[20−30] Due to the very high PLQY, we have used a confocal microscope to view the nanobelts. Figure 3L shows the fluorescence microscopic images of $CsPbI_3$ NBs after fresh synthesis, which clearly shows strong luminescence from the nanobelts.

2.3. Understanding the Mechanism of the Morphological Evolution from $CsPbI_3$ Nanocrystals to 1D $CsPbI_3$ Nanobelts Using Time-Dependent Microscopy Studies.

Due to the ionic nature of α-$CsPbI_3$ quantum dots, as well as the small binding energy of the surface ligands such as oleic acid (OA) and oleylamine (OAm), the bonding is highly dynamic in perovskite crystals.[2,3,14,20] Several publications indicate that OAm binds to the surface of the perovskite nanocrystals, but OA cannot bind to the surface of perovskite nanocrystals.[2,3,14−20] Most probably, OA formed a ligand pair with OAm.[2,3,14,20] Due to the cubic structure of α-$CsPbI_3$, as shown in Figures 1 and 2, nanocrystals do not possess a dipole moment. However, in the presence of 532 nm light, the electromagnetic field of the laser light induces a dipole on the α-$CsPbI_3$ via desorption of surface ligands. It is well documented that quantum confinement effects in nanocrystals increase the exciton (electron−hole pairs) binding energy and exciton radiative recombination.[2,3,11−20] Upon photoexcitation, the dissociation of electron−hole pairs into free charges is known to play an important role in the destabilization of surface stabilizers such as oleic acid (OA) and oleylamine (OAm) ligands.[2,3,14,20] To understand light-induced destabilization of surface stabilizers, we have performed IR spectroscopy on nanobelts, as reported in Figure 3G. FTIR data reported in Figure 3G clearly show the missing peak at 3310 cm^{-1}, which is due to $-NH_2$ group from oleylamine (OAm), and another missing peak at 1635 cm^{-1}, which is due to $-NH_3^+$ from protonated amine. Reported FTIR spectra indicate the desorption of OAm during the self-assembly process. To understand better, we have also performed high-resolution XPS analysis for α-$CsPbI_3$ nanocrystals and 1D $CsPbI_3$ nanobelts. As reported in Figure S3C in the Supporting Information, N 1s core level XPS spectra due to the protonated amine groups and oleylamine indicate the formation of efficiently detached the surface ligands during the light-induced synthesis of 1D $CsPbI_3$ nanobelts from nanocrystals.

Since surface halides bind to oleyl ammonium ions via hydrogen binding or electrostatic interactions, light can induce the formation of oleyl ammonium ions.[2,3,14,20] Excitons separated by the visible light can be captured by OA and OAm surface ligands on nanocrystals and destabilize the function of OAm and OA, which increases surface traps.[2,3,14,20] It is also reported that excess OAm in the solution can bind to the OA from neighboring $CsPbCl_3$ nanocrystals via the formation of OA−OAm pairs.[2,3,14,20] This ion-pair formation changes the neutrality of nanocrystals. This together with the dipole−dipole interactions helps to self-assemble the crystals with neighboring $CsPbI_3$ nanocrystals.[2,3,14,20] The structure distortion in the presence of 532 nm green light and induced polarization by the electromagnetic field of light reduced the

https://doi.org/10.1021/acsomega.3c00477
ACS Omega 2023, 8, 13202−13212

surface energy allowing the crystal phase transformation from cubic phase α-$CsPbI_3$ nanocrystals into orthorhombic perovskite γ-phase $CsPbI_3$ NBs.

To reveal the light-induced evolution process, we have performed a time dependent TEM and SEM study as shown in Figures 2B−F. TEM and SEM data show the formation process at different time points. Figure 2A shows the schematic representation of the formation of a $CsPbI_3$ nanobelt from $CsPbI_3$ nanocubes. As shown in Figure 2A, initially the $CsPbI_3$ nanocubes fused into a $CsPbI_3$ nanowire via the light-induced self-assembly process. The TEM image in Figure 2C shows that within 2 h, the $CsPbI_3$ nanotubes spontaneously aligned in the presence of light for the formation of the $CsPbI_3$ nanowire. Figure 2C,D shows the early formation stage of the $CsPbI_3$ nanowire via self-assembly of $CsPbI_3$ nanocrystals. The scheme of Figure 2A also shows that in the later stage, the $CsPbI_3$ nanowires fused into a $CsPbI_3$ nanobelt via side-by-side attachment through the light-induced self-assembly process. Figures 2E−G shows that at a later stage after 10 h, the $CsPbI_3$ nanowires were continuously assembled into nanobelts via a side-by-side aggregation process.

A reported DFT calculation shows that [001] and [110] surfaces are thermodynamically more stable than the [100] surface.[33] It also indicates that the thermodynamically most favorable nanowire formation should be via orientation of perovskite crystals along [001] facets with self-assembly growth along the [110] direction.[3,20,33] In our case, during the light-induced self-assembly process, nanowires initially grow along the [110] direction. Also, a recent report on vacancy-assisted regrowth indicates that the [100] surfaces have higher halogen-vacancy formation energy than the [110] surface, which allows the growth of nanowires along the [110] direction.[21] As a result, initially we observed the formation of a nanowire with length around 10 μm and diameter around 30 nm, as shown in Figure 2D. Excess illumination with visible light formed more and more OA−OAm pairs, which helped the formation of the nanobelt assembly via a self-organization process from 1D nanowires along the [001] direction and formed nanobelts, as shown Figure 2F,G. Recent DFT calculations show that compared with the (110) surface, the (001) possesses a lower surface energy.[3,20,33] As a result, although in the initial stage, the assembly grows along the [110] direction for the formation of nanowires, in the later stage the assembly of nanowires grows into nanobelts along the [001] direction.[3,20,33] Figure 2F clearly shows the self-assembly of nanowires. As reported in Figure 2G, we observed mostly 1D $CsPbI_3$ nanobelts after 12 h of illumination of light. The TEM data reported in Figure 2G indicates that the sizes of 1D $CsPbI_3$ nanobelts are around 10 ± 4 μm in length and 250 ± 40 nm in diameter.

2.4. Determining the Role of Light and Surface Ligands on the Morphological Evolution from $CsPbI_3$ Nanocrystals to 1D $CsPbI_3$ Nanobelts. Next, to determine the role of light absorption on the morphological evolution from nanocrystals to NBs, we have performed the same experiment with 785 and 910 nm laser sources, where $CsPbI_3$ nanocrystals do not have any absorption.

As reported in Figures S3 and S5 in the Supporting Information, the TEM data clearly indicate that we have not observed any formation of self-assembled 1D $CsPbI_3$ nanobelts even after 12 h of illumination with 785 or 910 nm light. All above data clearly indicate that light absorption by $CsPbI_3$ nanocrystals is an important step for the self-assembly process via generation of electron and hole separation and surface ligand desorption. The 532 nm laser power dependent study as reported in Figure 3H shows that 0.6 J/m^2 power of light is necessary to complete the process for the formation of nanobelts from nanocrystals. Similarly, the time dependent study, as reported in Figure 3I indicates that we need minimum 12 h to complete the formation of nanobelts from nanocrystals in the presence of 532 nm light.

To understand whether desorption of OAm the important step for anisotropic growth to NWs, we have performed additional experiments by adding excess OAm (0.060 mmol/mL) in $CsPbI_3$ nanocrystals solution just before the light-induced assembly process. From the time-resolved TEM experiment, we found out that in the presence of excess OAm, the formation of NBs happens in just 8 h, as shown in Figure S4 in the Supporting Information. On the other hand, without excess OAm, the formation of NBs happens in 12 hours, as shown in Figure 2. We have also observed that the length of the nanobelts can be enhanced from 10 ± 4 μm to 16 ± 3 μm by changing the amount of OAm from 0.060 mmol/mL to 0.09 mmol/mL. Similarly, we have also performed experiments with adding excess oleic acid (0.08 mmol/mL) into the $CsPbI_3$ nanocrystal solution just before the light-induced assembly process.

From the time-resolved TEM experiment, we found out that in the presence of excess OA, we did not find the formation of NBs and instead we found the formation of 2D nanoplates with the size of 30 ± 10 nm, as shown in Figure S4. We have also observed that nanoplate size can be increased by increasing the amount of OA. When we used 0.15 mmol/mL of OA, the 2D nanoplate size increased from 60 ± 10 nm to 100 ± 20 nm. Recently reported DFT calculation data indicated that during the light-induced desorption process, OA can detach much more easily than OAm.[2,4,14,20] As we have discussed, in case of 532 nm excitation, we have observed OAm detachment, and its presence is very important for the anisotropic growth from nanocrystals to nanowires.

To understand the role of light, we have also performed the same experiment without light in the presence of excess OAm (0.06 mmol/mL). As reported in Figure S10 in the Supporting Information, we have observed some amount of nanowire formation even after 20 days. All the above experimental data clearly indicate that OA presence is very important for the growth of nanoplates from nanocrystals. Also, the incident light plays an important role for growth kinetics in the formation of nanobelts from nanocrystals.

2.5. Determining the Phase and Air Stability of γ-$CsPbI_3$ Nanobelts. As we have discussed before, the phase transition from α-$CsPbI_3$ to non-perovskite yellow δ-$CsPbI_3$ phase in room temperature remains a major obstacle for commercial application.[1−10] To understand whether our design of γ-$CsPbI_3$ nanobelts exhibit phase and air stability, we have performed TEM/SEM, XRD, and photoluminescence spectra from the γ-$CsPbI_3$ nanobelts at different storage times. As shown in Figure S6 in the Supporting Information, TEM image of $CsPbI_3$ nanobelts after storage for 60 days shows same morphology as freshly prepared $CsPbI_3$ nanobelts as shown in Figure 2G.

Similarly, Figure 3F shows the X-ray diffraction patterns from $CsPbI_3$ NBs after fresh synthesis and storage for 60 days, which clearly indicate that orthorhombic phase for γ-$CsPbI_3$ nanobelts remains unchanged even after two months of storage. On the other hand, as shown in Figure 3E, the X-ray

https://doi.org/10.1021/acsomega.3c00477
ACS Omega 2023, 8, 13202−13212

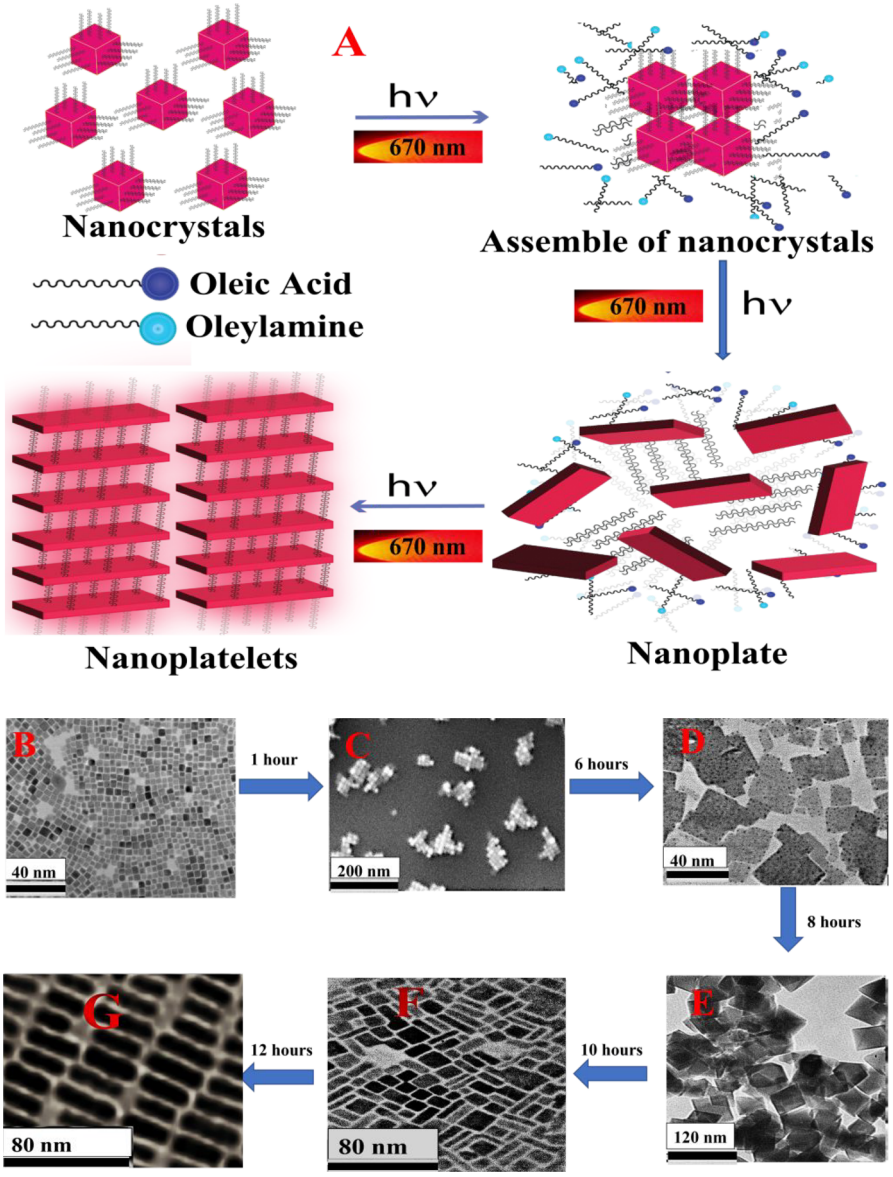

Figure 4. (A) Scheme showing 670 nm red light-induced evolution process from $CsPbI_3$ nanocrystals to γ-$CsPbI_3$ nanoplatelets (NPLs). (B−G) Time-resolved TEM and SEM data showing evidence of the evolution process from nanocrystals to nanoplatelets in the presence of 670 nm red light: (B) 0 h, (C) 1 h, (D) 6 h, (E) 8 h, (F) 10 h, and (G) 12 h.

diffraction data from α-$CsPbI_3$ after 30 days of storage show several XRD peaks which are due to the (012), (020), (021), (022), (014), (012), (015), (122), (016), (034), (035), (134), and (112) planes, which match with δ-$CsPbI_3$ phase. Reported XRD data indicate that the nanocrystals change from α-$CsPbI_3$ to non-perovskite yellow δ-$CsPbI_3$ phase within 30 days of storage.

Figure 3J,K shows the photoluminescence spectra from $CsPbI_3$ NBs after fresh synthesis and storage for 60 days, which clearly indicates that photoluminescence spectra remain unchanged even after two months of storing. On the other hand, as shown in Figure 3K, the photoluminescence intensity at 716 nm from α-$CsPbI_3$ changes abruptly just after few days of storage, which is due to the phase changes from α-$CsPbI_3$ to non-perovskite yellow δ-$CsPbI_3$ phase. Similarly, as shown in Figure 3L, the confocal microscope image shows strong luminescence from nanobelts even after 60 days of storage.

Steele et al.[39] have reported the use of interfacial clamping and strain to produce stable $CsPbI_3$ thin films at room temperature via thermodynamic trapping in an optically active black phase. In our case, the stability for orthorhombic phase for γ-$CsPbI_3$ nanobelts is due to the removal of a good amount of surface ligands from nanocrystals during the photoinduced self-assembly process. As we have discussed before, the light-induced self-assembly of $CsPbI_3$ nanocrystals occurs via light-induced desorption of surface ligands.[2,3,14] Upon photo-excitation, the dissociation of electron−hole pairs into free charge is known to play an important role for the destabilization of surface stabilizers such as oleic acid and oleylamine ligands.[2,3,13,30−39] The above process allows the removal of surface ligands from nanocrystals, which leads to opening vacancies in $CsPbI_3$ nanocrystals.[3,14,30−36] Due to the above fact, to fill these vacancies, $CsPbI_3$ nanocrystals undergo self-healing to deform and connect to each other. As a result, we have observed $CsPbI_3$ nanocrystal to $CsPbI_3$ nanobelt

https://doi.org/10.1021/acsomega.3c00477
ACS Omega 2023, 8, 13202−13212

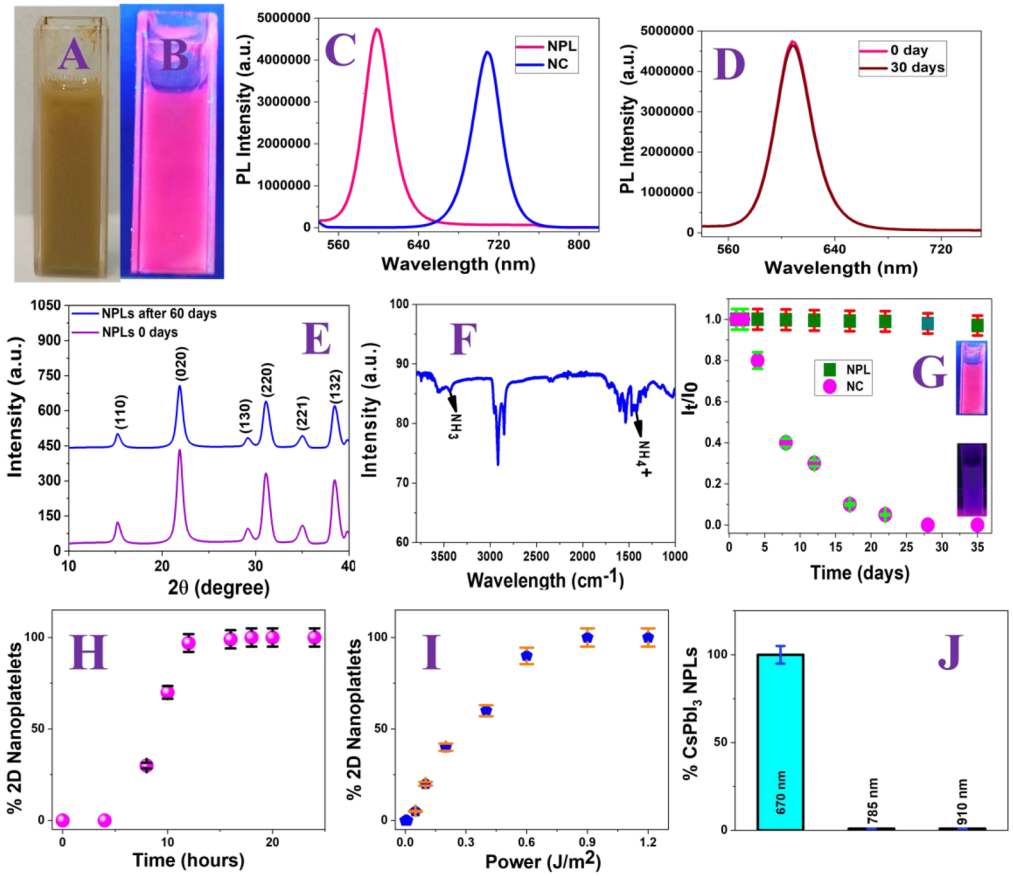

Figure 5. (A) Photograph of $CsPbI_3$ NPL in the absence of UV light. (B) Photograph of $CsPbI_3$ NPLs in the presence of UV light. (C) Photoluminescence spectra of $CsPbI_3$ nanocrystals and NPLs. (D) Photoluminescence spectra of $CsPbI_3$ NPLs at 0 and 60 days. (E) X-ray diffraction patterns from $CsPbI_3$ NPLs after fresh synthesis and storage for 30 days show γ-$CsPbI_3$ (JCPDS No. 18-0376) in both cases. (F) FTIR spectra from $CsPbI_3$ NPLs. (G) Plot shows how the luminescence intensity from $CsPbI_3$ nanocrystals and $CsPbI_3$ NPLs varies with the storage time in normal temperature. The experiment was performed five times, and error bars were calculated from the standard deviation. (H) Plot shows the variation of % of $CsPbI_3$ NPL formation with the power (J/m^2) of 670 nm visible light. The experiment was performed five times, and error bars were calculated from the standard deviation. (I) Plot shows the variation of % of $CsPbI_3$ NPL formation with time during the 670 nm light-induced self-assembly process. The experiment was performed five times, and error bars were calculated from the standard deviation. (J) Plot shows how the 2D nanoplatelet formation varies with the excitation wavelength of light. The experiment was performed five times, and error bars were calculated from the standard deviation.

formation via transforming the morphologies and phases. Reported FTIR spectra in Figure 3G and N 1s core level XPS spectra in Figure S3C in the Supporting Information show that efficient detachment of surface ligands occurs during the light-induced assembly process for nanocrystal to nanobelt formation.

Also, in the assembled structure, nanocrystals are assembled into close-packed structures. As a result, the surface ligands are mostly tightly bonded in γ-$CsPbI_3$ nanobelts.[30−39] As we have discussed before, in the presence of electromagnetic field of 532 nm green light, ion-pair formation changes the neutrality of nanocrystals. As a result, self-assembly of the crystals with neighboring $CsPbI_3$ nanocrystals happens via dipole−dipole interactions.[2,3,14,20] Due to this process, $CsPbI_3$ nanocrystals are assembled into close-packed structures in $CsPbI_3$ nanobelts, which allow the surface ligands to be tightly bonded. Due to the presence of less surface ligands and tightly bonded ligands, γ-$CsPbI_3$ nanobelts exhibit higher stability in comparison to $CsPbI_3$ nanocrystals.

2.6. 670 nm Red Light Driven Synthesis, Characterization, and Photochemistry of γ-$CsPbI_3$ Nanoplatelets from α-$CsPbI_3$ Nanocrystals. For light driven synthesis of nanoplatelets from nanocrystals, we have used a 670 nm DPSS laser as light source. For this experiment, we used 100 mW/cm^2 laser power for the development of NPLs via assembly of $CsPbI_3$ nanocrystals. As shown in Figure 4, upon exposure to 670 nm light for several hours, $CsPbI_3$ nanocrystals transform into nanoplates initially and then to 2D $CsPbI_3$ nanoplatelets. As shown in Figure 4G, the TEM data indicate that the size of 2D $CsPbI_3$ nanoplatelets are around 20 ± 6 nm in length and 4 ± 1 nm in thickness. As shown in Table 1, the DLS data also matches with the TEM data. Energy-dispersive X-ray (EDX) spectroscopy (Figure S7 in Supporting Information) and inductively coupled plasma mass spectrometer (ICP-MS) data indicate that the NPLs are $CsPbI_3$. X-ray diffraction (XRD) data, as reported in Figure 5E, shows (110), (020), (130), (220), (221), and (132) planes for NPLs, which indicates orthorhombic phase for γ-$CsPbI_3$ nanoplatelets.[12−14] From XRD data reported in Figure 5E,F, we can clearly see the phase change from α-$CsPbI_3$ nanocrystals to γ-$CsPbI_3$ NPLs. Similarly, the HRTEM image, as shown in the inset image of Figure 1, shows clear lattice fringes with interplanar spacing (d) of ∼0.26 nm, which is due to the (220) crystal plane of γ-$CsPbI_3$.[12−14] Figure 5A shows the photograph of γ-$CsPbI_3$

https://doi.org/10.1021/acsomega.3c00477
ACS Omega 2023, 8, 13202−13212

nanoplatelets in the absence of UV light. Figure 5B shows the photograph of γ-$CsPbI_3$ nanoplatelets in the presence of UV light, which clearly shows strong orange luminescence. Figure 5C shows the luminescence spectra from γ-$CsPbI_3$ nanoplatelets, which indicates that photoluminescence λ_{max} of freshly prepared NPL is 605 nm. From the emission spectra of $CsPbI_3$ nanocrystals and $CsPbI_3$ NPLs, we can clearly observe a huge blue shift of λ_{max} from 716 to 605 nm. The observed photoluminescence blue shift for 2D $CsPbI_3$ NPLs compared with the 3D $CsPbI_3$ nanocrystals can be due to the stronger quantum confinement, because of the low thickness of 4 ± 1 nm.[21,26,27] It is now well documented that the photoluminescence λ_{max} for $CsPbI_3$ NPLs varies with the thickness.[21,26,27] In our case, the dimension of γ-CsPbI3 was reduced to n = 1 to n = 3, which also contributed to the observed huge blue shift of photoluminescence λ_{max} for 2D $CsPbI_3$ NPLs.[21,26,27] The photoluminescence quantum yield measurement shows that PLQY increases from 88% to 91% after self-assembly formation from $CsPbI_3$ nanocrystals to γ-$CsPbI_3$ nanoplatelets. As we have observed in the SEM/TEM images reported in Figure 4 the dense arrangement of nanocrystals to 2D $CsPbI_3$ NPLs via certain disorder, which can help localization of excitons in the local potential minima.[20−30] As a result, the traps formed in the presence of light may not heavily involve recombination processes, which enhances PLQY for 2D $CsPbI_3$ NPLs in comparison to $CsPbI_3$ nanocrystals.[20−30] To understand better, we have measured photoluminescence lifetimes for nanocrystals and nanoplatelets as reported in Table S1A in the Supporting Information. Reported photoluminescence lifetime data indicate that for nanocrystals photoluminescence carrier lifetime is ∼3 ns and on the other hand for nanoplatelets photoluminescence carrier lifetime is ∼75 ns. This observed longer photoluminescence carrier lifetime for nanoplatelets in comparison to nanocrystals indicates effective suppression of nonradiative traps for nanoplatelets and it also indicates long carrier diffusion length for nanoplatelets.[20−30] So experimentally observed higher PLQY for the assembled structure can be due to the low trap density and strong quantum confinement.[20−30]

2.7. Understanding the Mechanism of the Morphological Evolution from $CsPbI_3$ Nanocrystals to 2D $CsPbI_3$ Nanoplatelets Using Time-Dependent Microscopy Studies. As we have discussed before, in the presence of light, the electro-magnetic field of laser light induces a dipole on the α-$CsPbI_3$ via desorption of surface ligands. In the presence of 670 nm light, the dissociation of electron−hole pairs plays an important role for the destabilization of surface stabilizers.[2,3,14,20] To understand this process, we have performed IR spectroscopy from nanoplatelets as reported in Figure 5F. FTIR data reported in Figure 5F clearly shows the small peak at 3310 cm^{-1}, which is due to $-NH_2$ group from oleyl amine (OAm) and another small peak at 1635 cm^{-1}, which is due to $-NH_3^+$, from protonated amine. As we have reported before, in the case of 532 nm self-assembly process for the formation of nanobelts, the IR peaks for $-NH_2$ group and $-NH_3^+$ groups are missing. In comparison, from the FTIR data reported in Figures 3G and 5F, it is clear that desorption of OAm during the self-assembly process is smaller in case of the 670 nm light based self-assembly process than the 532 nm light-induced self-assembly process. To understand better, we have also performed high resolution XPS analysis for α-$CsPbI_3$ nanocrystals and 2D $CsPbI_3$ nanoplatelets. As reported in Figure S3D in the Supporting Information, N 1s core level XPS spectra due to the protonated amine groups and oleylamine indicates that detached surface ligands occur during the light-induced synthesis of 2D $CsPbI_3$ nanoplatelets from nanocrystals.

As we have discussed before, recently reported DFT calculation data indicate that during light-induced desorption processes, OA can detach much more easily than OAm.[2,4,14,20] Since OAm detachment and its presence are very important for the anisotropic growth from nanocrystal, due to the lack of a good amount of OAm, the nanocrystals growth into nanoplatelets. The structure distortion in the presence of 670 nm red light and induced polarization by the electromagnetic field of light reduced the surface energy, which allows the crystal phase transformation from cubic phase α-$CsPbI_3$ nanocrystals into orthorhombic perovskite γ-phase $CsPbI_3$ NPLs.

To reveal the light-induced evolution process, we have performed a time dependent TEM study, as shown in Figure 4B−G. TEM data show the formation process at different time points as we have reported in Figure 4A. As shown in Figure 4C, with just 2 h of illumination we have observed destabilization of some $CsPbI_3$ nanocrystals and started formation of $CsPbI_3$ nanoplate. Reported DFT calculation shows that [001] and [110] surfaces are thermodynamically more stable than [100] surface,[33] and as a result, $CsPbI_3$ nanocrystals evolve into nanoplates along the [110] and [001] directions, which can be seen in Figure 4A,D. Excess illumination of visible light destabilized more and more ligands, which helps in the formation of nanoplatelets via a self-organization process from nanoplates along the [001] direction and formed nanoplatelets, as shown Figure 4F,G. As reported in Figure 4G, we observed mostly 2D $CsPbI_3$ nanoplates after 12 h of illumination with 670 nm red light.

2.8. Determining the Role of Light and Surface Ligands on the Morphological Evolution from $CsPbI_3$ Nanocrystals to 2D $CsPbI_3$ Nanoplatelets. Next, to determine the role of light absorption on the morphological evolution from nanocrystals to NPLs, we have performed the same experiment with 785 and 910 nm laser source, where $CsPbI_3$ nanocrystals do not have any absorption. As reported in Figure S8 in the Supporting Information, the TEM data clearly indicate that we have not observed any formation of self-assembled 2D $CsPbI_3$ nanoplatelets even after 12 h of illumination with 785 or 910 nm light. All above data clearly indicate that light absorption by $CsPbI_3$ nanocrystals is an important step for the self-assembly process via generation of electron and hole separation and surface ligand desorption. The 670 nm laser power dependent study as reported in Figure 5H shows that 0.9 J/m^2 power of light is necessary to complete the process for the formation of nanoplatelets from nanocrystals. Similarly, the time dependent study, as reported in Figure 5I, indicates that we need a minimum of 12 h to complete the formation of nanoplatelets from nanocrystals in the presence of 670 nm light.

To understand whether desorption of surface ligands such as OA and OAm is the important step for the growth to nanoplatelets, we have performed additional experiments by adding excess OAm to $CsPbI_3$ nanocrystals solution just before the 670 nm light-induced assembly process. From the time-resolved TEM experiment, we found out that in the presence of excess OAm (0.060 mmol/mL) the formation of nanorods with length of 160 ± 40 nm happens in 12 hours via anisotropic growth along one direction as shown in Figure S9 in the Supporting Information. We have also observed that the

https://doi.org/10.1021/acsomega.3c00477
ACS Omega 2023, 8, 13202−13212

length of the nanorods can be enhanced from 160 ± 40 nm to 220 ± 40 nm by changing the amount of OAm from 0.060 mmol/mL to 0.1 mmol/mL. At the same condition, we have observed nanobelts with the length of 16 ± 3 μm when the excitation wavelength was 532 nm. To understand the role of light, we have also performed the same experiment without light in the presence of excess OAm (0.060 mmol/mL). As reported in Figure S10 in the Supporting Information, we have observed some nanowire formation even after 20 days. All the above experimental data clearly indicate that OAm presence is very important for the anisotropic growth from nanocrystal to nanowire. Also, the incident light plays an important role for growth kinetics for the formation of nanorods, nanowires, and nanobelts from nanocrystals via anisotropic growth of nanocrystals.

Similarly, we have also performed experiments by adding excess oleic acid OA (0.08 mmol/mL) to $CsPbI_3$ nanocrystals solution just before the 670 nm light-induced assembly process. From the time-resolved TEM experiment we found out that in the presence of excess OA we see the formation of NPLs, as shown in Figure S9 in the Supporting Information. The reported experimental data clearly indicate that OA presence is very important for the growth from nanocrystal to NPLs. As we have reported before, in the case of 532 nm excitation, the desorption of OAm is higher than that from 670 nm excitation, which allows the formation of nanobelts via anisotropic growth along one direction. On the other hand, with the lack of OAm destabilization in the case of 670 nm light excitation, OA allows the formation of nanoplatelets. To understand the role of light, we have also performed the same experiment without light in the presence of excess OA (0.08 mmol/mL). As reported in Figure S10 in the Supporting Information, we have observed some amount of nanoplates even after 20 days. All the above experimental data clearly indicate that OA presence is very important for the growth of nanoplates from nanocrystals. Also, the incident light plays an important role for growth kinetics for the formation of nanoplate and nanoplatelets from nanocrystals.

2.9. Determining the Phase and Air Stability of γ-$CsPbI_3$ Nanoplatelets. As we have discussed before, the phase transition from α-$CsPbI_3$ to non-perovskite yellow δ-$CsPbI_3$ phase in room temperature remains a major obstacle for commercial application.[1−10] To understand whether our design of γ-$CsPbI_3$ nanoplatelets exhibits phase and air stability, we have performed TEM/SEM, XRD, and photoluminescence spectra from the γ-$CsPbI_3$ nanoplatelets at different storage times. As shown in Figure S11 in the Supporting Information, the TEM image of $CsPbI_3$ nanoplatelets after storage for 60 days shows the same morphology as freshly prepared $CsPbI_3$ nanoplatelets, as shown in Figure 4G.

Similarly, Figure 5E shows the X-ray diffraction pattern from $CsPbI_3$ nanoplatelets after fresh synthesis and storage for 60 days, which clearly indicates that orthorhombic phase for γ-$CsPbI_3$ nanoplatelets remains unchanged even after two months of storage. On the other hand, as shown in Figure 3E, the X-ray diffraction data show that the nanocrystals change from α-$CsPbI_3$ to non-perovskite yellow δ-$CsPbI_3$ phase within 30 days of storage. Figure 5D,G show the photoluminescence spectra from $CsPbI_3$ NBs after fresh synthesis and storage for 60 days, which clearly indicates that the photoluminescence spectra remain unchanged even after two months of storage. On the other hand, as shown in Figure 3K, the photoluminescence intensity at 716 nm from α-$CsPbI_3$ changes abruptly just after few days of storage, which is due to the phase changes from α-$CsPbI_3$ to non-perovskite yellow δ-$CsPbI_3$ phase.

Reported high stability for orthorhombic phase for $CsPbI_3$ nanoplatelets is due to the removal of a good amount of surface ligands from nanocrystals during the photoinduced self-assembly process. As we have discussed before, in the case of the 670 nm light-induced assembly process, the dissociation of electron−hole pairs into free charge helps the destabilization of surface ligands.[2,3,13,30−39] The above process allows the removal of surface ligands from nanocrystals. Reported FTIR spectra in Figure 5F and N 1s core level XPS spectra in Figure S3D in the Supporting Information show that detachment of surface ligands happens during the light-induced assembly process from nanocrystals to nanoplatelets. Also, in the assembled structure of γ-$CsPbI_3$ nanoplatelets, nanocrystals are assembled into close-packed structures leading to mostly tightly bonded structures in γ-$CsPbI_3$ nanoplatelets.[30−39] Due to the presence of less surface ligands and tightly bonded ligands, γ-$CsPbI_3$ nanoplatelets exhibit higher stability in comparison to $CsPbI_3$ nanocrystals.

3. CONCLUSIONS

In conclusion, our findings reveal that visible-light-induced self-assembly formation of $CsPbI_3$ nanocrystals into targeted 2D nanoplatelets and 1D nanowires can be manipulated by varying the excitation wavelength. Reported experimental data show that 532 nm green light-driven self-assembly produces phase stable and highly luminescent γ-$CsPbI_3$ nanobelts from $CsPbI_3$ nanocrystals. On the other hand, experimental data indicates that the 670 nm red light-driven self-assembly process produces stable and near unity PLQY γ-$CsPbI_3$ NPLs. Systematic time dependent SEM and TEM imaging shows the possible pathway for the formation of 1D γ-$CsPbI_3$ nanobelts and 2D γ-$CsPbI_3$ nanoplatelets from α-$CsPbI_3$ nanocrystals.

Experimental study of the morphological evolution indicates that the electromagnetic field of light triggered the desorption of surface ligands from nanocrystal surface and transformation of crystallographic phase from α to γ. Detached OAm and OA ligands help to achieve the morphologies of final structures of NBs and NPLs from nanocrystals via oriented attachment along the [110] direction and [001] direction. From the reported data, we found out that at 532 nm excitation the detachment of OAm process is higher than that at 670 nm excitation, which allows formation of nanobelt via anisotropic growth to nanowire along the [110] direction and then growth of nanobelt from nanowire along [001] direction. Experimental data show that the 532 nm incident light plays an important role for growth kinetics for the formation of 1D nanowire and nanobelts from nanocrystals via anisotropic growth. On the other hand, the detachment of OAm is much lower in case of 670 nm light excitation, and as a result, OA allows the formation of nanoplatelets. Reported data indicate that for this self-assembly process, initially $CsPbI_3$ nanocrystals evolved into nanoplates along the [110] and [001] directions and after that nanoplatelets formed via a self-organization process from nanoplates along [001] direction. Experimental data show that 670 nm incident light plays an important role for growth kinetics for the formation of nanoplates and nanoplatelets. Using XRD and fluorescence imaging, our experimental data indicate that both NBs and NPLs exhibit phase stability for

https://doi.org/10.1021/acsomega.3c00477
ACS Omega 2023, 8, 13202−13212

more than 60 days in ambient conditions, whereas the cubic phase α-$CsPbI_3$ nanocrystals are not stable for even 3 days. Undoubtedly, reported data demonstrated that light is crucial to achieving the ordered assembly formation process, and it is a powerful approach for controlling the structure, shape, phase, and dimensions of $CsPbI_3$ perovskites.

Due to the low trap density, strong quantum confinement, and enhanced stability, 532 nm green light-driven self-assembly based 1D γ-$CsPbI_3$ nanobelts and 670 nm red light-driven self-assembly based 2D γ-$CsPbI_3$ nanoplatelets can be suitable candidates for advanced lighting and photoelectric device applications. Due to the stronger absorption in the solar spectrum, higher PLQY, and longer photoluminescence carrier lifetime, γ-$CsPbI_3$ nanobelts will be a better choice for photovoltaic and photoelectric devices in comparison to 2D γ-$CsPbI_3$ nanoplatelets. Although we have reported that visible-light-induced self-assembly formation is a powerful approach for controlling the shape of 1D γ-$CsPbI_3$ nanobelts and 2D γ-$CsPbI_3$ nanoplatelets, it is fair to acknowledge that full understanding on the driving forces which control the assembly process is still in its infancy. We really need to understand the interaction between the light electric field, surface ligands, and nanomaterials which control the self-assembly structure. This is important before they can be used in practical optoelectronic applications.

■ ASSOCIATED CONTENT

Supporting Information

The Supporting Information is available free of charge at https://pubs.acs.org/doi/10.1021/acsomega.3c00477.

Design and characterization of $CsPbI_3$ crystals, nanobelts, and nanoplates (PDF)

■ AUTHOR INFORMATION

Corresponding Author

Paresh Chandra Ray − *Department of Chemistry and Biochemistry, Jackson State University, Jackson, Mississippi 39217, United States;* orcid.org/0000-0001-5398-9930; Email: paresh.c.ray@jsums.edu; Fax: +16019793674

Authors

Avijit Pramanik − *Department of Chemistry and Biochemistry, Jackson State University, Jackson, Mississippi 39217, United States;* orcid.org/0000-0002-4623-2099

Sudarson Sekhar Sinha − *Department of Chemistry and Biochemistry, Jackson State University, Jackson, Mississippi 39217, United States;* orcid.org/0000-0002-0831-2338

Kaelin Gates − *Department of Chemistry and Biochemistry, Jackson State University, Jackson, Mississippi 39217, United States*

Jing Nie − *Department of Chemistry and Biochemistry, Jackson State University, Jackson, Mississippi 39217, United States*

Fengxiang X Han − *Department of Chemistry and Biochemistry, Jackson State University, Jackson, Mississippi 39217, United States;* orcid.org/0000-0001-5135-3031

Complete contact information is available at: https://pubs.acs.org/10.1021/acsomega.3c00477

Notes

The authors declare no competing financial interest.

■ ACKNOWLEDGMENTS

Dr. Ray thanks NSF-PREM, grant no. DMR-1826886, for their generous funding. We also thank NIH-NIMHD, grant no. 1U54MD015929-01 for the core facility.

■ REFERENCES

(1) Li, Z.; Fan, Q.; Yin, Y. Colloidal Self-Assembly Approaches to Smart Nanostructured Materials. *Chem. Rev.* **2022**, *122*, 4976−5067.

(2) Chen, J.; Zhou, Y.; Fu, Y.; Pan, J.; Mohammed, O. F.; Bakr, O. M. Oriented Halide Perovskite Nanostructures and Thin Films for Optoelectronics. *Chem. Rev.* **2021**, *121*, 12112−12180.

(3) Liu, J.; Zheng, X.; Mohammed, O. F.; Bakr, O. M. Self-Assembly and Regrowth of Metal Halide Perovskite Nanocrystals for Optoelectronic Applications. *Acc. Chem. Res.* **2022**, *55*, 262−274.

(4) García de Arquer, F. P.; Talapin, D. V.; Klimov, V. I.; Arakawa, Y.; Bayer, M.; Sargent, E. H. Semiconductor quantum dots: Technological progress and future challenges. *Science* **2021**, *373*, No. eaaz8541.

(5) Cherniukh, I.; Raino, G.; Stoferle, T.; Burian, M.; Travesset, A.; Naumenko, D.; Amenitsch, H.; Erni, R.; Mahrt, R. F.; Bodnarchuk, M. I.; Kovalenko, M. V. Perovskite-type superlattices from lead halide perovskite nanocubes. *Nature* **2021**, *593*, 535−542.

(6) Ke, F.; Wang, C.; Jia, C.; Wolf, N. R.; Yan, J.; Niu, S.; Devereaux, T. P.; Karunadasa, H. I.; Mao, W. L.; Lin, Y. Preserving a Robust $CsPbI_3$ Pervoskite Phase via Pressure-Directed Octahedral Tilt. *Nat. Commun.* **2021**, *12*, 461.

(7) Mir, J. W.; Alamoudi, A.; Yin, J.; Yorov, K. E.; Maity, P.; Naphade, R.; Shao, B.; Wang, J.; Lintangpradipto, M. N. S.; Nematulloev, S.; Emwas, A. H.; Genovese, A.; Mohammed, O. F.; Bakr, O. M. Lecithin Capping Ligands Enable Ultrastable Perovskite-Phase CsPbI3 Quantum Dots for Rec. 2020 Bright-Red Light-Emitting Diodes. *J. Am. Chem. Soc.* **2022**, *144* (29), 13302−13310.

(8) Bera, S.; Banerjee, S.; Das, R.; Pradhan, N. Tuning Crystal Plane Orientation in Multijunction and Hexagonal Single Crystalline $CsPbBr_3$ Perovskite Disc Nanocrystals. *J. Am. Chem. Soc.* **2022**, *144*, 7430−7440.

(9) Dubose, J. T.; Kamat, P. V. Energy Versus Electron Transfer: Managing Excited-State Interactions in Perovskite Nanocrystal-Molecular Hybrids. *Chem. Rev.* **2022**, *122*, 12475−12494.

(10) Dubose, J. T.; Kamat, P. V. TiO_2-Assisted Halide Ion Segregation in Mixed Halide Perovskite Films. *J. Am. Chem. Soc.* **2020**, *142*, 5362−5370.

(11) Zhao, B.; Jin, S. F.; Huang, S.; Liu, N.; Ma, J. Y.; Xue, D. J.; Han, Q.; Ding, J.; Ge, Q. Q.; Feng, Y.; Hu, J. S. Thermodynamically Stable Orthorhombic gamma-$CsPbI_3$ Thin Films for High-Performance Photovoltaics. *J. Am. Chem. Soc.* **2018**, *140*, 11716−11725.

(12) Duan, L.; Zhang, H.; Liu, M.; Grätzel, M.; Luo, J. Phase-Pure γ-CsPbI3 for Efficient Inorganic Perovskite Solar Cells. *ACS Energy Letters* **2022**, *7*, 2911−2918.

(13) Sun, J. K.; Huang, S.; Liu, X. Z.; Xu, Q.; Zhang, Q. H.; Jiang, W. J.; Xue, D. J.; Xu, J. C.; Ma, J. Y.; Ding, J.; Ge, Q. Q.; Gu, L.; Fang, X. H.; Zhong, H. Z.; Hu, J. S.; Wan, L. J. Polar Solvent Induced Lattice Distortion of Cubic $CsPbI_3$ Nanocubes and Hierarchical Self-Assembly into Orthorhombic Single-Crystalline Nanowires. *J. Am. Chem. Soc.* **2018**, *140*, 11705−11715.

(14) Paul, S.; Acharya, S. Postsynthesis Transformation of Halide Perovskite Nanocrystals. *ACS Energy Letters* **2022**, *7*, 2136−2155.

(15) Lan, Y.-F.; Yao, J.-S.; Yang, J.-N.; Song, Y.-H.; Ru, X.-C.; Zhang, Q.; Feng, L.-Z.; Chen, T.; Song, K.-H.; Yao, H.-B. Spectrally Stable and Efficient Pure Red $CsPbI_3$ Quantum Dot Light-Emitting Diodes Enabled by Sequential Ligand Post-Treatment Strategy. *Nano Lett.* **2021**, *21*, 8756−8763.

(16) Straus, D. B.; Guo, S.; Cava, R. J. Kinetically Stable Single Crystals of Perovskite-Phase CspbI3. *J. Am. Chem. Soc.* **2019**, *141*, 11435−11439.

(17) Jana, A.; Meena, A.; Patil, S. A.; Jo, Y.; Cho, S.; Park, Y.; Sree, V. G.; Kim, H.; Im, H.; Taylor, R. A. Self-assembly of perovskite nanocrystals. *Prog. Mater. Sci.* **2022**, *129*, 100975.

(18) Dubose, J. T.; Christy, A.; Chakkamalayath, J.; Kamat, P. V. Transformation of Perovskite Nanoplatelets to Large Nanostructures Driven by Solvent Polarity. *ACS Mater. Lett.* **2022**, *4*, 93−101.
(19) Pan, J.; Shang, Y.; Yin, J.; De Bastiani, M.; Peng, W.; Dursun, I.; Sinatra, L.; El-Zohry, A. M.; Hedhili, M. N.; Emwas, A.-H.; Mohammed, O. F.; Ning, Z.; Bakr, O. M. Bidentate Ligand-Passivated $CsPbI_3$ Perovskite Nanocrystals for Stable near-Unity Photoluminescence Quantum Yield and Efficient Red Light-Emitting Diodes. *J. Am. Chem. Soc.* **2018**, *140*, 562−565.
(20) Liu, J.; Song, K.; Shin, Y.; Liu, X.; Chen, J.; Yao, K. X.; Pan, J.; Yang, C.; Yin, J.; Xu, L.-J.; Yang, H.; El-Zohry, A. M.; Xin, B.; Mitra, S.; Hedhili, M. N.; Roqan, I. S.; Mohammed, O. F.; Han, Y.; Bakr, O. M. Light-Induced Self-Assembly of Cubic $CsPbBr_3$ Perovskite Nanocrystals into Nanowires. *Chem. Mater.* **2019**, *31*, 6642−6649.
(21) Pan, J.; Li, X.; Gong, X.; Yin, J.; Zhou, D.; Sinatra, L.; Huang, R.; Liu, J.; Chen, J.; Dursun, I.; El-Zohry, A. M.; Saidaminov, M. I.; Sun, H.-T.; Mohammed, O. F.; Ye, C.; Sargent, E. H.; Bakr, O. M. Halogen Vacancies Enable Ligand-Assisted Self-Assembly of Perovskite Quantum Dots into Nanowires. *Angew. Chem., Int. Ed.* **2019**, *131*, 16223−16227.
(22) Bekenstein, Y.; Koscher, B. A.; Eaton, S. W.; Yang, P. D.; Alivisatos, A. P. Highly Luminescent Colloidal Nanoplates of Perovskite Cesium Lead Halide and Their Oriented Assemblies. *J. Am. Chem. Soc.* **2015**, *137*, 16008−16011.
(23) Liu, Y.; Siron, M.; Lu, D.; Yang, J.; dos Reis, R.; Cui, F.; Gao, M.; Lai, M.; Lin, J.; Kong, Q.; Lei, T.; Kang, J.; Jin, J.; Ciston, J.; Yang, P. Self-Assembly of Two-Dimensional Perovskite Nanosheet Building Blocks into Ordered Ruddlesden-Popper Perovskite Phase. *J. Am. Chem. Soc.* **2019**, *141*, 13028−13032.
(24) Polavarapu, L.; Vila-Liarte, D.; Feil, M. W.; Manzi, A.; Garcia-Pomar, J. L.; Huang, H.; Doblinger, M.; Liz-Marzan, L. M.; Feldmann, J.; Mihi, A. Templated-Assembly of $CsPbBr_3$ Perovskite Nanocrystals into 2D Photonic Supercrystals with Amplified Spontaneous Emission. *Angew. Chem., Int. Ed.* **2020**, *59*, 17750−17756.
(25) Paul, S.; Samanta, A. Phase-Stable and Highly Luminescent CsPbI3 Perovskite Nanocrystals with Suppressed Photoluminescence Blinking. *J. Phys. Chem. Lett.* **2022**, *13* (25), 5742−5750.
(26) Pramanik, A.; Patibandla, S.; Gao, Y.; Gates, K.; Ray, P. C. Water Triggered Synthesis of Highly Stable and Biocompatible 1D Nanowire, 2D Nanoplatelet, and 3D Nanocube CsPbBr3 Perovskites for Multicolor Two-Photon Cell Imaging. *J. Am. Chem. Soc. Au* **2021**, *1*, 53−65.
(27) Wang, K.; Li, Z.; Zhou, F.; Wang, H.; Bian, H.; Zhang, H.; Wang, Q.; Jin, Z.; Ding, L.; Liu, S. Ruddlesden-Popper 2D Component to Stabilize γ-CsPbI3 Perovskite Phase for Stable and Efficient Photovoltaics. *Adv. Energy Mater.* **2019**, *9*, 1902529.
(28) Bi, C.; Hu, J.; Yao, Z.; Lu, Y.; Binks, D.; Sui, M.; Tian, J. Self-Assembled Perovskite Nanobelt Clusters for High Luminance Red Light-Emitting Diodes. *Adv. Funct. Mater.* **2020**, *30*, 2005990.
(29) An, Y.; Hidalgo, J.; Perini, C. A. R.; Castro-Méndez, A.-F.; Vagott, J. V.; Bairley, K.; Wang, S.; Li, X.; Correa-Baena, J.-P. Structural Stability of Formamidinium- and Cesium-Based Halide Perovskites. *ACS Energy Lett.* **2021**, *6*, 1942−1969.
(30) Ji, Y.; Wang, M.; Yang, Z.; Qiu, H.; Kou, S.; Padhiar, M. A.; Bhatti, A. S.; Gaponenko, N. V. Pressure-Driven Transformation of $CsPbBrI_2$ Nanoparticles into Stable Nanosheets in Solution through Self-Assembly. *J. Phys. Chem. Lett.* **2020**, *11*, 9862−9868.
(31) Pramanik, A.; Gates, K.; Patibandla, S.; Davis, D.; Begum, S.; Iftekhar, R.; Alamgir, S.; Paige, S.; Porter, M. M.; Ray, P. C. Water-Soluble and Bright Luminescent Cesium-Lead-Bromide Perovskite Quantum Dot-Polymer Composites for Tumor-Derived Exosome Imaging. *ACS Appl. Bio Mater.* **2019**, *2*, 5872−5879.
(32) Pramanik, A.; Gates, K.; Gao, Y.; Begum, S.; Chandra Ray, P. Several Orders-of-Magnitude Enhancement of Multiphoton Absorption Property for CsPbX3 Perovskite Quantum Dots by Manipulating Halide Stoichiometry. *J. Phys. Chem. C* **2019**, *123*, 5150−5156.
(33) Liu, J.; Song, K.; Zheng, X.; Yin, J.; Yao, K. X.; Chen, C.; Yang, H.; Hedhili, M. N.; Zhang, W.; Han, P.; Mohammed, O. F.; Han, Y.; Bakr, O. M. Cyanamide Passivation Enables Robust Elemental Imaging of Metal Halide Perovskites at Atomic Resolution. *J. Phys. Chem. Lett.* **2021**, *12*, 10402−10409.
(34) Dong, Y.; Wang, Y. K.; Yuan, F.; Johnston, A.; Liu, Y.; Ma, D.; Choi, M. J.; Chen, B.; Chekini, M.; Baek, S. W.; Sagar, L. K.; Fan, J.; Hou, Y.; Wu, M.; Lee, S.; Sun, B.; Hoogland, S.; Quintero-Bermudez, R.; Ebe, H.; Todorovic, P.; Dinic, F.; Li, P.; Kung, H. T.; Saidaminov, M. I.; Kumacheva, E.; Spiecker, E.; Liao, L. S.; Voznyy, O.; Lu, Z. H.; Sargent, E. H. Bipolar-shell resurfacing for blue LEDs based on strongly confined perovskite quantum dots. *Nat. Nanotechnol.* **2020**, *15*, 668−674.
(35) Ma, D.; Lin, K.; Dong, Y.; Choubisa, H.; Proppe, A. H.; Wu, D.; Wang, Y.-K.; Chen, B.; Li, P.; Fan, J. Z.; Yuan, F.; Johnston, A.; Liu, Y.; Kang, Y.; Lu, Z.-H.; Wei, Z.; Sargent, E. H. Distribution Control Enables Efficient Reduced-Dimensional Perovskite LEDs. *Nature* **2021**, *599*, 594−598.
(36) Kim, Y. H.; Kim, S.; Kakekhani, A.; Park, J.; Park, J.; Lee, Y. H.; Xu, H.; Nagane, S.; Wexler, R. B.; Kim, D. H.; Jo, S. H.; Martínez-Sarti, L.; Tan, P.; Sadhanala, A.; Park, G. S.; Kim, Y. W.; Hu, B.; Bolink, H. J.; Yoo, S.; Friend, R. H.; Rappe, A. M.; Lee, T. W. Comprehensive defect suppression in perovskite nanocrystals for high-efficiency light-emitting diodes. *Nat. Photonics.* **2021**, *15*, 148−155.
(37) Kim, J. S.; Heo, J.-M.; Park, G.-S.; Woo, S.-J.; Cho, C.; Yun, H. J.; Kim, D.-H.; Park, J.; Lee, S.-C.; Park, S.-H.; Yoon, E.; Greenham, N. C.; Lee, T.-W. Ultra-Bright, Efficient and Stable Perovskite LightEmitting Diodes. *Nature* **2022**, *611*, 688−694.
(38) Hassan, Y.; Park, J. H.; Crawford, M. L.; Sadhanala, A.; Lee, J.; Sadighian, J. C.; Mosconi, E.; Shivanna, R.; Radicchi, E.; Jeong, M.; et al. Ligand-engineered bandgap stability in mixed-halide perovskite LEDs. *Nature* **2021**, *591*, 72−77.
(39) Steele, J. A.; Jin, H. D.; Dovgaliuk, I.; Berger, R. F.; Braeckevelt, T.; Yuan, H. F.; Martin, C.; Solano, E.; Lejaeghere, K.; Rogge, S. M. J.; et al. Thermal unequilibrium of strained black $CsPbI_3$ thin films. *Science* **2019**, *365*, 679−684.
(40) Wang, S.; Yousefi Amin, A. A.; Wu, L.; Cao, M.; Zhang, Q.; Ameri, T. Perovskite Nanocrystals: Synthesis, Stability, and Optoelectronic Applications. *Small Struct.* **2021**, *2*, 2000124.
(41) Jana, A.; Cho, S.; Patil, S. A.; Meena, A.; Jo, Y.; Sree, V. G.; Park, Y.; Kim, H.; Im, H.; Taylor, R. A. Perovskite: Scintillators, direct detectors, and X-ray imagers. *Mater. Today* **2022**, *55*, 110.

https://doi.org/10.1021/acsomega.3c00477
ACS Omega 2023, 8, 13202−13212